Open Access Online Journal on Astronomy and Astrophysics

Acta Astrophysica Taurica

www.astrophysicatauricum.org

Acta Astrophys. Tau. 5(2), 17–20 (2024)

Determining the parameters of the low accretion rate polar V379 Vir

M.V. Suslikov[1], A.I. Kolbin[1,2]

[1] Kazan (Volga Region) Federal University, Kremlyovskaya 18, Kazan 420008, Russian Federation
e-mail: mvsuslikov@outlook.com

[2] Special Astrophysical Observatory of the Russian Academy of Sciences, Nizhnij Arkhyz 369167, Karachai-Cherkessian Republic, Russian Federation
e-mail: kolbinalexander@mail.ru

Received 26 October 2021

ABSTRACT

This paper presents a determination of the parameters of the low accretion rate polar V379 Vir. Using data from the ground-based and space observatories, we obtained the spectral energy distribution in a wide spectral range, corrected for interstellar absorption. Modeling this distribution allowed us to determine the mass and effective temperature of the white dwarf: $M_1 = 0.628 \pm 0.009\ M_\odot$, $T_{\rm eff} = 11250 \pm 70$ K. Based on the semi-amplitude of the radial velocities of the secondary component's irradiated surface, we estimated its mass $M_2 \approx 0.027\ M_\odot$ and the inclination of the orbital plane $i = 50 \pm 5°$.

Key words: cataclysmic variables, novae, stars: individual: V379 Vir

1 Introduction

Polars (AM Her-type variables) are close binary systems consisting of a white dwarf with a strong magnetic field (primary component, $B \sim 10^7$–10^8 MG) and a cold main-sequence dwarf filling its Roche lobe (secondary component). The material from the secondary component outflows from the Lagrange point L_1 region into the primary component's Roche lobe and initially moves along a trajectory close to ballistic. The strong magnetic field of the white dwarf prevents the formation of an accretion disk. After reaching the Alfvén radius of the primary component, where the ram pressure of the accretion flow becomes equal to the magnetic pressure ($\rho v^2 = B^2/8\pi$), the ionized gas is captured by the magnetic field lines and moves toward the magnetic poles. The accreting gas with supersonic speed falls onto the surface of the white dwarf and forms a shock front at heights of ~0.01–0.1 accretor radii. In post-shock region, the gas heats up to high temperatures ($T \sim$ 10–50 keV), forming the accretion column on the surface of the white dwarf. The main cooling mechanisms are bremsstrahlung and cyclotron radiation in the optical range.

To understand the origin and characteristics of the evolution of polars, it is important to determine the physical parameters of stellar components. However, solving this issue has many difficulties. At high accretion rates the integral emission of the system is overwhelmingly contributed by the accretion flow and accretion column and makes it practically impossible to estimate the system's parameters based on optical observations. The best conditions are achieved when the system transitions to a low accretion state. However, even in the case when the components of the system are visible in the spectrum, the determination of their parameters is a difficult task. Thus, the spectral lines of the white dwarf are split by the quadratic Zeeman effect, complicating the measurement of its radial velocities. The radial velocities of the secondary component are strongly affected by the inhomogeneity of the brightness distribution over the stellar surface. The orbital movement of the secondary component is often manifested only in emission lines formed on the irradiated surface of the star.

In the present work, we performed a determination of the parameters of the low accretion rate polar V379 Vir. The first studies of this system (Schmidt et al., 2005) identified it as an interacting short-period variable with a magnetic white dwarf and a brown dwarf. The authors obtained the average magnetic field of the white dwarf of 7 MG and also detected periodic variability of the radial velocity of Hα emission ($P \approx$ 90 min), formed in the irradiated region on the secondary component. Burleigh et al. (2006) detected photometric variability with the same period, but in antiphase with the radial velocity curve of the Hα line, and pointed to the presence of a shock region on the surface of the white dwarf. Subsequently, Debes et al. (2006) identified excess radiation in the near-infrared range, which indicates the presence of a cold brown dwarf of spectral type L5 – L7 with a photosphere temperature of less than 1700 K. The light curve in the K_s band exhibits variability with a period of ≈ 88 min, caused by the cyclotron radiation of the shock region on the white dwarf's surface. Further spectral studies in the near-infrared range (Farihi et al., 2008) confirmed the presence of a late L-type brown dwarf. Analysis of XMM-Newton observations

in the X-ray range (Stelzer et al., 2017) revealed a weak accretion rate of about 10^{-14} $M_\odot$/yr. In this work, we performed modeling of the spectral energy distribution of V379 Vir and determined the parameters of the white dwarf. In addition, based on the radial velocity curve of Hα emission, we estimated the parameters of the secondary component and inclination.

2 Spectral energy distribution of V379 Vir

Photometric observations of V379 Vir were performed with ground-based and space observatories in a wide wavelength range. Observations in the visible and near-infrared ranges were obtained by SDSS (Szkody et al., 2011) and VISTA telescope (Edge et al., 2013). Ultraviolet fluxes were obtained at the Swift UVOT and GALEX telescopes.

When constructing the spectral energy distribution of V379 Vir, the interstellar absorption was taken into account. It is known that the apparent magnitude of the source decreases due to interstellar absorption and scattering. The dependence of absorption on wavelength $A(\lambda)$ causes a decrease in brightness in the short-wave range the most, leading to the reddening of the source (Trumpler, 1930). The reddening is usually expressed through the color excess $E(B-V)$. The interstellar extinction in the photometric band x and the color excess are related by the well-known expression

$$R_x = \frac{A_x}{E(B-V)}, \qquad (1)$$

where R_x is the extinction coefficient of the passband x.

To determine $E(B-V)$ for the studied object, the relation between this parameter and the column density of neutral hydrogen in the line of sight was used. Bohlin et al. (1978) examined the absorption of interstellar neutral hydrogen in the Galaxy near the spectral line $L\alpha$. They showed that the average ratio between the column density HI and the color excess $E(B-V)$ is constant:

$$\left\langle \frac{N_{\rm HI}}{E(B-V)} \right\rangle = 4.8 \times 10^{21} \text{ atoms cm}^{-2} \text{ mag}^{-1}. \qquad (2)$$

Based on modeling of the X-ray data of V379 Vir, Stelzer et al. (2017) obtained the column density of neutral hydrogen in the line of sight, $N_{\rm HI} = 2.3 \times 10^{20}$ atoms cm^{-2}. Using this value and according to formula (2), the color excess $E(B-V) = 0.048$ was calculated for V379 Vir. Extinction coefficients for the SDSS and VISTA photometric systems were determined in Yuan et al. (2013) and Gonzalez-Fernandez et al. (2018), respectively. Using these values and the previously calculated color excess $E(B-V)$ in equation (1), we obtained the corrections A_x taking into account interstellar absorption in optics for SDSS and VISTA magnitudes. Observational data of V379 Vir from Swift UVOT and GALEX in the ultraviolet range already take interstellar absorption into account.

The determination of parameters was performed using the synthetic photometry. Since the primary and secondary components mainly contribute to the emission of the polar in a low state, then the total flux f_ν of the system was found by adding the spectra of the white and brown dwarfs. For the white dwarf, the intensities were calculated based on the stationary plane-parallel LTE models of stellar atmospheres (Koester, 2010). Having fixed the white dwarf's gravitational acceleration at $\log g = 8.0$, estimated through photometric observations (Schmidt et al., 2005), a grid of spectra was obtained for a set of effective temperatures $T_{\rm eff}$. The secondary component was taken into account by adding the template spectrum of the L8-type star 2MASS J16322911+1904407. The spectral type L8 produced best fitting of the observed infrared spectra (Farihi et al., 2008).

The observed spectral energy distribution was described by the least squares method involving the minimization of the function

$$\chi^2(\theta, T_{\rm eff}) = \sum_k^l \left(\frac{\theta^2 f_k(T_{\rm eff}) - f_k^{\rm obs}}{\sigma_k} \right)^2, \qquad (3)$$

where θ is the angular radius of the source in radians; f_k and $f_k^{\rm obs}$ are the theoretical and the observed flux, respectively; σ_k are the photometric errors; and the index k corresponds to the photometric band. During the minimization process of expression (3), the angular radius and the effective temperature of the white dwarf were found.

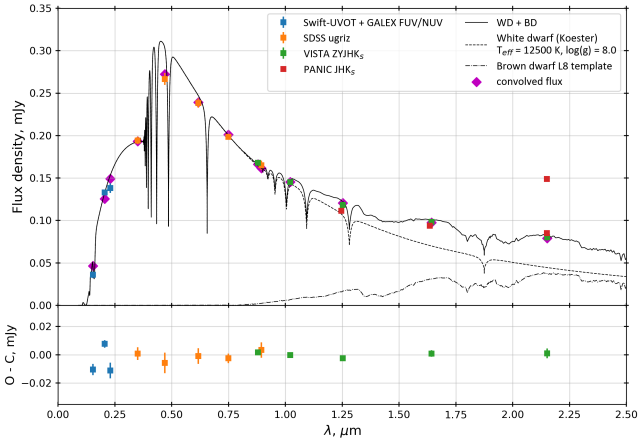

Fig. 1. Spectral energy distribution of V379 Vir.

Since the emission of the primary component dominates in the optical and ultraviolet spectral range, a more accurate approximation was performed with the single model spectrum of the white dwarf in the photometric fluxes of Swift UVOT, GALEX, and SDSS. The result of the best fitting of the observed spectral energy distribution by the model of the white dwarf is represented by the dashed line in Fig. 1. The fitting model of the white dwarf spectrum has the temperature $T_{\rm eff} = 11250 \pm 70$ K. The angular radius of the primary component was also obtained to be $\theta = 3.754 \times 10^{-7} \pm 0.032 \times 10^{-7}$″. To perform the approximation of the VISTA infrared fluxes to the white dwarf model, a spectrum of the L8 brown dwarf was added. The resulting integrated spectrum is represented by the solid line in Fig. 1. The deviation of the observed fluxes from the synthetic ones according to the O–C diagram is less than 0.2 mJy, indicating good agreement of the two-component model with observations. Averaged fluxes from the light curves in the JHK$_s$ bands obtained by Debes et al. (2006) corrected for extinction were also plotted. From the K$_s$ light curve, we obtained two flux

density values: by averaging magnitudes in the phase interval $\Delta\phi = 0.8 - 1.2$ with constant emission from the secondary component and in the interval $\Delta\phi = 0.2 - 0.8$ corresponding to the appearance of a source of cyclotron radiation. The Monte Carlo method was applied to estimate the parameters errors found from the fitting of the observed spectral energy distribution.

3 Determining the component parameters

From the previously obtained angular radius of the primary component and the parallax of V379 Vir $\pi = 6.68 \times 10^{-3} \pm 0.18 \times 10^{-3}{''}$ from the GAIA DR3 catalog (Gaia Collaboration, 2018), the radius of the white dwarf was determined to be $R_1 = 0.0121 \pm 0.0001\ R_\odot$. It is well known that the mass – radius relation for white dwarfs was analytically expressed by Nauenberg (1972) as

$$R_1 = 7.795 \times 10^8 \left[\left(\frac{1.44 M_\odot}{M_1} \right)^{2/3} - \left(\frac{M_1}{1.44 M_\odot} \right)^{2/3} \right]^{1/2} \text{cm}. \quad (4)$$

Solving this equation gives an estimate of the white dwarf's mass $M_1 = 0.628 \pm 0.009\ M_\odot$. The corresponding surface gravity of the primary component is $\log g = 8.07$, which is well agreed with the estimation in Schmidt et al. (2005) ($\log g = 8.0$).

In the spectral analysis of V379 Vir performed by Schmidt et al. (2005), the radial velocity curve for the Hα line emission was obtained. The source of this emission is considered to be the secondary component's surface irradiated by the X-ray emission from the accretion spot. The authors estimated the semi-amplitude of the radial velocity curve for this region to be $K_2' = 320 \pm 20$ km/s. However, to estimate the star's parameters, it is necessary to find the semi-amplitude of the radial velocities for the center of mass K_2. The semi-amplitude K_2 was identified by us through modeling the X-ray irradiated atmosphere of the cold star facing the accretor (see Shimanskii et al., 2012). The modeling assumed that the secondary component's rotation is synchronized with its orbital motion. The X-ray luminosity of the accretion spot was set to be $L_X = 3{\times}10^{29}$ erg/s (Stelzer et al., 2017), and the shape of the spectral distribution in the X-ray range was supposed according to Cropper (1990). Theoretical radial velocities of the Hα emission were measured using the cross-correlation method in 72 phases of the orbital period. Based on these measurements, the correction for the semi-amplitude of the radial velocity was calculated to be $\Delta K_2 = K_2 - K_2' = 26.8 \pm 1.3$ km/s.

Using photometric observations in Debes et al. (2006), we refined the orbital period of the system $P_{\rm orb} = 0.^d060781$ by applying the Lafler – Kinman method. The mass function $f(M_2)$ was calculated according to the formula

$$f(M_2) = 1.0385 \times 10^{-7} (P_{\rm orb} K_2^3) \quad (5)$$

and found to be $f(M_2) = 0.263 \pm 0.049\ M_\odot$. On the other hand, it is known that

$$f(M_2) = \frac{M_1^3 \sin^3 i}{(M_1 + M_2)^2}, \quad (6)$$

where M_1 is the mass of the white dwarf, M_2 is the mass of the secondary component, and i is the inclination of the orbital plane.

Additional constraints needed to determine the parameters of the V379 Vir components can be obtained from the assumption that the secondary component is close to filling its Roche lobe. According to Eggleton (1983), the effective radius R_L of the Roche lobe of the secondary component can be estimated as

$$\frac{R_L}{A} = 0.49 \frac{q^{2/3}}{0.6 q^{2/3} + \ln(1 + q^{1/3})}, \quad (7)$$

where $q = M_2/M_1$ is the mass ratio of the secondary to the primary component, and A is the separation of the mass centers of the components. A can be calculated using Kepler's third law: $A = (M_1(1+q)P_{\rm orb}^2)^{1/3}$.

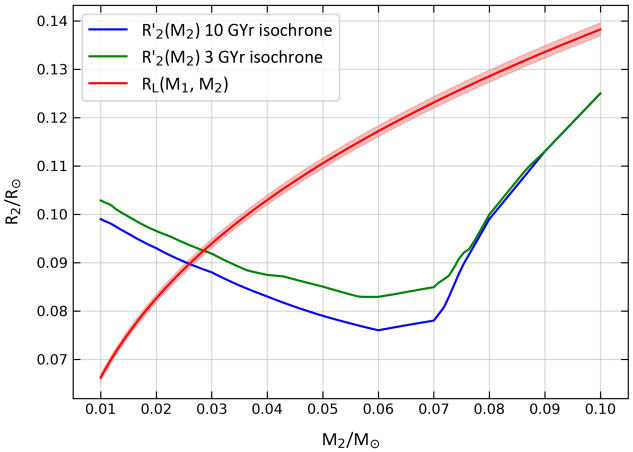

Fig. 2. Evolutionary radius – mass relations for brown dwarfs corresponding to ages of 3×10^9 and 10^{10} years (green and blue lines, respectively), as well as the effective Roche lobe radius of the secondary component (red line).

Meanwhile, the radius of the secondary component is related to its mass by the evolutionary relation $R_2'(M_2)$. This relation was obtained from the isochrones in Baraffe et al. (2003) for the solar abundances ($Z = 0.019$). By limiting the system's age between $t_1 = 3 \times 10^9$ and $t_2 = 10^{10}$ years and solving the equation $R_2'(M_2) = R_L(M_2, M_1)$ for the two specified ages, we found the mass of the secondary component to be $M_2 = 0.027 \pm 0.001\ M_\odot$ (approximately 28.5 Jupiter masses) and its effective radius to be $R_2 \approx 0.091\ R_\odot$. A graphical representation of the evolutionary relations $R_2'(M_2)$ and the effective Roche lobe radius $R_L(M_2, M_1)$ for $M_1 = 0.628 \pm 0.009\ M_\odot$ is given in Fig. 2.

Inserting the found masses of the components into expression (6) gives the inclination of the orbital plane $i = 50 \pm 5°$. From Kepler's third law, the separation between components $A = 0.565 \pm 0.003\ R_\odot$ is obtained. Solving the system of equations for the mass function of the primary component $f(M_1)$, we find the semi-amplitude of the radial velocity curve for the white dwarf $K_1 = 15.1 \pm 0.7$ km/s. All found parameters and errors are listed in Table 1.

Table 1. Parameters of the V379 Vir system.

Parameter	Value	Error
$T_{\rm eff}$, K	11250	70
$\log g$	8.07	
$P_{\rm orb}$, days	0.060781	
π, $\times 10^{-3}$ arcsec	6.68	0.18
d, pc	149	4
i, degrees	50	5
K_1, km/s	15.1	0.7
K_2, km/s	346.8	21.3
R_1, $R_\odot$	0.0121	0.0001
R_2, $R_\odot$	0.091	0.001
M_1, $M_\odot$	0.628	0.009
M_2, $M_\odot$	0.027	0.001
A, $R_\odot$	0.565	0.003

4 Conclusions

In this work, we have carried out a photometric study of the polar V379 Vir, which is in a low accretion rate state. By using the results of observations from various ground-based and space observatories in a wide wavelength range, we constructed the spectral energy distribution of V379 Vir corrected for interstellar extinction. By fitting the observed fluxes with the model spectra of the white dwarf and the L8 brown dwarf, an estimate of the primary component's temperature was obtained to be $T_{\rm eff} = 11\,250 \pm 70$ K. Based on the known GAIA parallax and the angular size of the primary component, its radius was determined to be $R_1 = 0.0120 \pm 0.0001\ R_\odot$ and mass $M_1 = 0.628 \pm 0.009\ M_\odot$. Using the semi-amplitude of the radial velocity curve of the irradiated region on the secondary component K_2' and assuming that the donor fills its Roche lobe, we estimated the inclination of the orbital plane to be $i = 50 \pm 5^\circ$, as well as the mass and radius of the secondary component to be $M_2 \approx 0.027\ M_\odot$ and $R_2 \approx 0.091\ R_\odot$, respectively.

Acknowledgments. This research was supported by the Russian Foundation for Basic Research as part of the scientific project No. 19-32-60048.

References

Baraffe I., Chabrier G., Barman T.S., et al., 2003. Astron. Astrophys., vol. 402, pp. 701–712.
Bohlin R.C., Savage B.D., Drake J.F., 1978. Astrophys. J., vol. 224, pp. 132–142.
Burleigh M.R., Marsh T.R., Gansicke B.T., et al., 2006. Mon. Not. Roy. Astron. Soc., vol. 373, pp. 1416–1422.
Cropper M., 1990. Space Sci. Rev., vol. 54, pp. 195–295.
Debes J.H., Lopez-Morales M., Bonanos A.Z., et al., 2006. Astrophys. J., vol. 647, pp. 147–150.
Edge A., Sutherland W., Viking Team, 2013. VizieR On-line Data Catalog: II/343.
Eggleton P.P., 1983. Astrophys. J., vol. 268, pp. 368–369.
Farihi J., Burleigh M.R., Hoard D.W., 2008. Astrophys. J., vol. 674, pp. 421–430.
Gaia Collaboration, 2018. VizieR On-line Data Catalog: I/345.
Girardi L., Bressan A., Bertelli G., et al., 2000. Astron. Astrophys. Suppl. Ser., vol. 141. pp. 371–383.
Gonzalez-Fernandez C., Hodgkin S.T., Irwin M.J., et al., 2018. Mon. Not. Roy. Astron. Soc., vol. 474, pp. 5459–5478.
Koester D., 2010. Memorie della Societa Astronomica Italiana, vol. 81. pp. 921–931.
Nauenberg M., 1972. Astrophys. J., vol. 175, p. 417.
Schmidt G.D., Szkody P., Silvestri N.M., et al., 2005. Astrophys. J., vol. 630, pp. 173–176.
Shimanskii V.V., Karitskaya E.A., Bochkarev N.G., et al., 2012. Astron. Rep, vol. 56, pp. 741–760.
Stelzer B., de Martino D., Casewell S.L., et al., 2017. Astron. Astrophys., vol. 598, p. 6.
Szkody P., Anderson S.F., Brooks K., et al., 2011. Astron. J., vol. 142, p. 9.
Trumpler R.J., 1930. Lick Observatory Bulletin, vol. 420. pp. 154–188.
Yuan H.B., Liu X.W., Xiang M.S., 2013. Mon. Not. Roy. Astron. Soc., vol. 430, pp. 2188–2199.